Freestanding graphene networks

C. A. BANCIU*, D. PATROI, E. M. LUNGULESCU, B. G. SBARCEA, V. E. MARINESCU
National Institute for Research and Development in Electrical Engineering ICPE-CA Bucharest, 313 Splaiul Unirii, sector 3, Bucharest – 030138, Romania

Graphene is an allotrope of carbon in the form of a single layer of atoms that presents special properties, of interest for electronic, optoelectronic, and energy storage applications. In this paper, we prepare flexible freestanding graphene networks using nickel foam as substrate in a chemical vapour deposition process with methane as carbon source. Different deposition times were used to obtain graphene with thicknesses from few-layer to multilayer, the controlled number of layers being an important aspect for their use in various applications. After nickel etching, the freestanding graphene networks were investigated by SEM, EDS, XRD and Raman spectroscopy.

(Received September 24, 2020; accepted April 8, 2021)

Keywords: Freestanding graphene, 3D networks, Chemical vapour deposition, Nickel foam

1. Introduction

Graphene, a monolayer of carbon atoms packed hexagonally into a 2D structure, has many superior physical and chemical properties, which make it highly attractive for numerous and various applications [1-7].

In recent years, researchers focused on obtaining a graphene structure in which individual sheets of graphene are bonded together to form a three-dimensional network. This prevents re-packing of individual graphene sheets in order to maintain intrinsic properties of graphene in the bulk structure and to increase the use of graphene in practical applications. In this regard, researchers turned their attention to develop by different methods three-dimensional graphene networks with various morphologies, structures, and properties [8-11]. Such three-dimensional (3D) structures were reported in literature and included graphene aerogels, graphene sponges and graphene foams [12, 13]. Graphene aerogels are usually obtained by sol-gel method to reduce graphene oxide in order to form a highly cross-linked graphene hydrogel, followed by water removal [14, 15]. Graphene foams were synthesized for the first time in 2011 by Chen et al. using nickel foam as template [16]. Thus, the graphene foam preserved the 3D geometry of the original nickel foam, forming a continuous and interconnected 3D graphene network. Graphene sponges have a porous structure with graphene sheets being partially oriented or aligned nearly parallel with each other, creating an anisotropic lamellar structure [17]. Graphene sponges have highly efficient and recyclable absorption performance [18, 19].

These 3D structures reveal new properties such as high specific surface areas, strong mechanical strengths and fast mass and electron transport kinetics, possessing the properties combination of the 3D porous structures and graphene. 3D structures can be used in many fields as absorbents, catalysis, sensors, in energy storage and conversion and biological applications [12, 13, 20-25].

In this work, the three-dimensional graphene layer was developed by thermal chemical vapour deposition (CVD) on commercial nickel foam which has a double role, as catalyst for graphene growth and as three-dimensional scaffold [16, 26, 27]. In order to obtain the freestanding graphene networks, the nickel foam was removed by a chemical etching process. After the complete nickel removal, the graphene layer preserved the 3D geometry of the original metal foam. We used different deposition times in order to determine the best configuration regarding the thickness of the graphene sheet and maintaining the structural integrity of the graphene network. The freestanding three-dimensional graphene structures were investigated by SEM, EDS, XRD and Raman spectroscopy. The obtained graphene structures are intended to be used subsequently as flexible electrodes in different applications, such as dye sensitized solar cells or carbon-based photodetectors. Thus, the obtaining of three-dimensional graphene with a controlled number of layers is an important aspect for their integration in different devices.

2. Materials and methods

The graphene layer was synthesized from a gas mixture of methane, hydrogen and argon on nickel foam catalyst produced by Gelon LIB Group China, using thermal CVD method at atmospheric pressure in a horizontal furnace (EasyTube 2000, FirstNano, CVD Equipment Corporation, USA). The high purity gases used for the graphene growth, methane (> 99.9995 %), hydrogen (> 99.995 %), and argon (> 99.999 %), were used as received from SIAD Romania. The characteristics of the nickel foam were the following: the porosity of 110 PPI (pores-per-inch), the thickness lower than 2.5 mm and the density higher than 250 g/m^2.

The thermal CVD growth of the 3D graphene layer was performed on nickel foam substrates with dimensions of 5 cm x 5 cm, ultrasonically cleaned in acetone and isopropyl alcohol before being placed into the CVD furnace [20, 26, 27]. The Ni foam was annealed for 15 minutes under argon and hydrogen atmosphere at 1000°C in order to remove any nickel oxide that could be present on the foam surface. After this, the growth process took place by adding the methane as carbon source. The process was carried out for 5, 7, 10, 15, 30 minutes in a gas mixture of $3.33 \cdot 10^{-6}$ $m^3 \cdot s^{-1}$ CH_4, $5.42 \cdot 10^{-6}$ $m^3 \cdot s^{-1}$ H_2 and $1.67 \cdot 10^{-5}$ $m^3 \cdot s^{-1}$ Ar. The holder containing the samples was retracted from the heated furnace area into a sealed chamber, where they were rapidly cooled to room temperature under Ar and H_2 protective atmosphere. The freestanding 3D graphene samples were obtained by etching the nickel foam in an aqueous solution of HCl (3 M) at a temperature of 80°C around 10 h.

Hereinafter, the graphene layer grown on the nickel foam, before etching the nickel foam substrate, will be referred to as GN-Ni, and the freestanding graphene networks will be referred to as GN.

The morphology of the freestanding graphene networks was observed using an Auriga Station Scanning Electron Microscope (SEM) from Carl Zeiss at different magnifications.

Energy-dispersive X-ray spectroscopy (EDS) analysis was conducted using an energy dispersive spectrometer with X-Max^N Silicon Drift Detector with active area of 50 mm^2 and software AZtec for acquisition and interpretation, made by Oxford Instruments UK.

X-ray diffraction (XRD) was conducted using a Bruker D8Discover diffractometer, configured in θ-2θ geometry, equipped with Cu anode (λ=1.5406Å) and 1D LynxEye detector. The diffractograms were recorded at 40 kV, 40 mA, with an angular increment of 0.04°, step time of 1s/step, in the angular range of 23°-70°. Qualitative identification was performed using ICDD PDF2 Release 2015 database after instrument error correction.

Raman spectroscopy was performed using a dispersive Horiba Raman Spectrometer, model LabRAM HR Evolution, in order to identify the structural defects of the freestanding graphene networks and to determine the number of layers in the graphene. An excitation laser with the wavelength of 532 nm and a low power of 12.5 mW was used in order to avoid the sample heating. The Raman spectra were acquired in the spectral range of 800-3400 cm^{-1} at an acquisition time of 15 seconds with 10 accumulations/spectrum using a diffraction grating with 600 grooves/mm and 50x objective lens with numerical aperture of 0.75.

3. Results and discussions

A series of graphene samples were synthesized by CVD on a scaffold of porous nickel foam using different deposition times. The nickel foam deposited with the graphene layer was cut in square samples of 1.5 x 1.5 cm. The nickel scaffold was then removed using chemical etching by a hot HCl solution. A continuous 3D network of graphene layer formed as a freestanding macroscopic structure with thin interconnected graphene sheets was obtained (Figure 1a, 1b). Graphene layers synthesized at short deposition times, 5-10 minutes (GN5, GN7, GN10), collapsed during nickel foam etching, while graphene layers synthesized at longer deposition times, 15 and 30 minutes (GN15, GN30), maintained their integrity. The GN replicated the interconnected 3D scaffold structure of the initial nickel foam substrate. The graphene layers have grown on the entire surface of the nickel foam substrate and so they are interconnected with each other. The obtained GNs are porous, flexible, and light-weight.

(a)

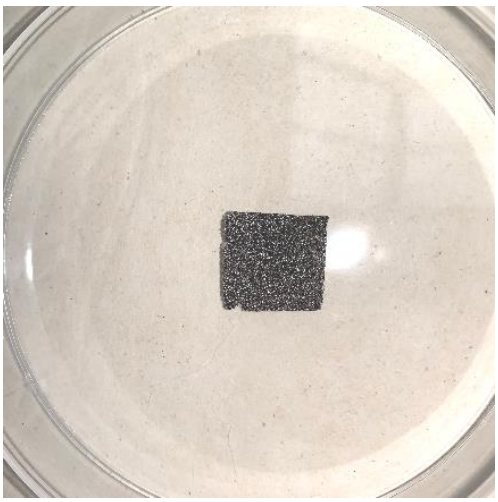

(b)

Fig. 1. Freestanding graphene networks: a) GN10, b) GN15 (color online)

Fig. 2 (a-e) illustrates scanning electron microscopy (SEM) images to reveal the morphology of the freestanding graphene networks microstructure.

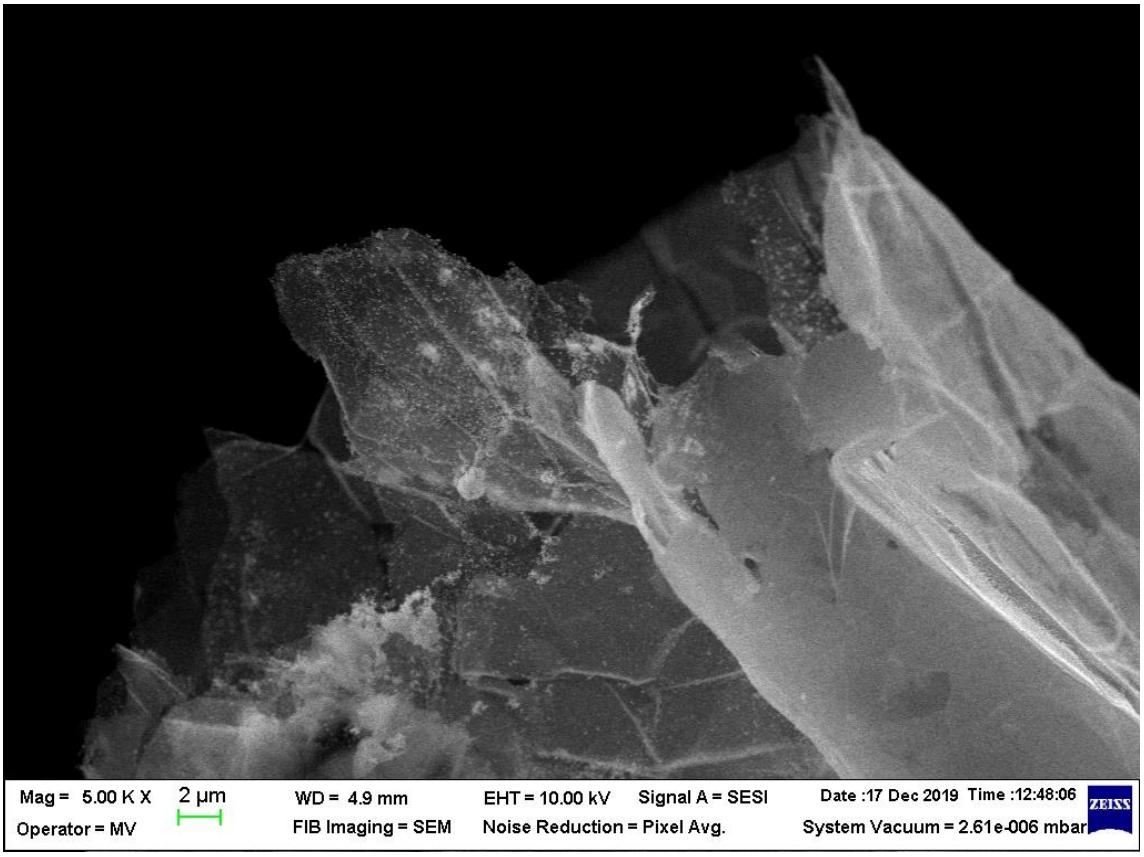
Mag = 5.00 K X
2 µm
WD = 4.9 mm
EHT = 10.00 kV
Signal A = SESI
Date :17 Dec 2019 Time :12:48:06
Operator = MV
FIB Imaging = SEM
Noise Reduction = Pixel Avg.
System Vacuum = 2.61e-006 mbar
ZEISS

(a)

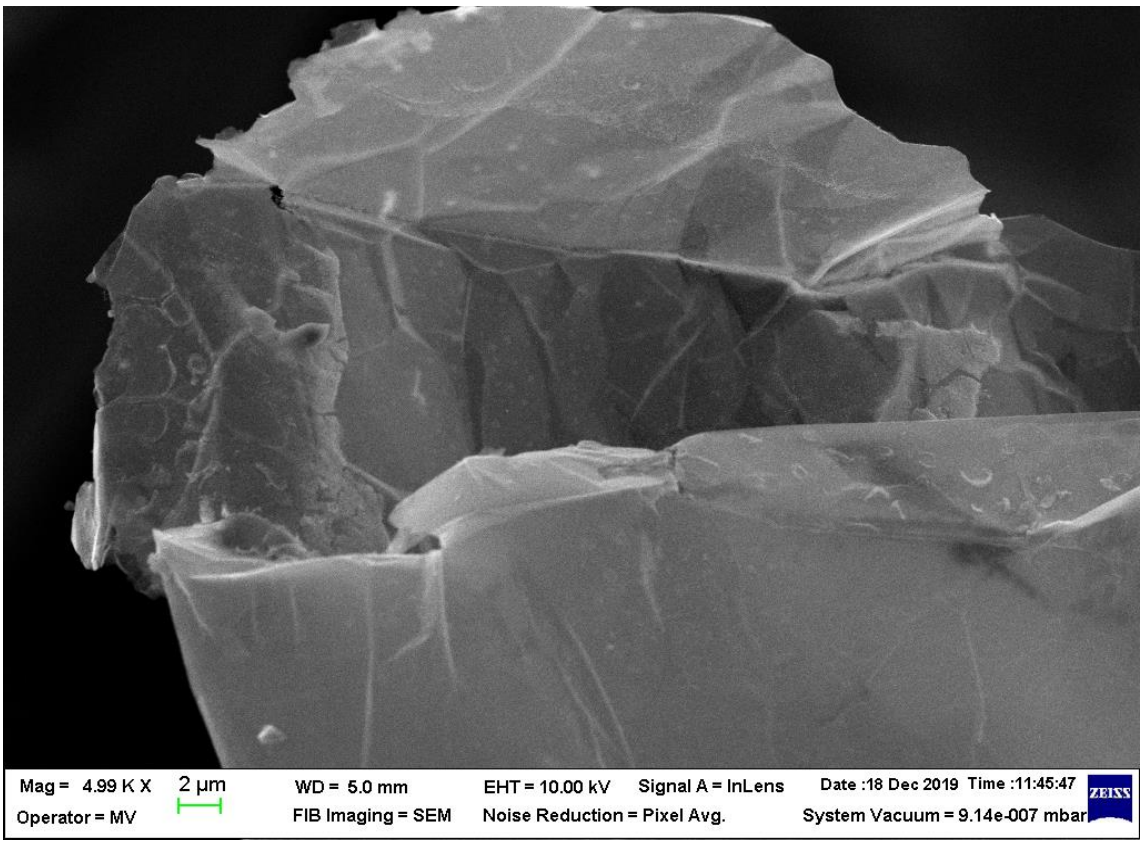
Mag = 4.99 K X
2 µm
WD = 5.0 mm
EHT = 10.00 kV
Signal A = InLens
Date :18 Dec 2019 Time :11:45:47
Operator = MV
FIB Imaging = SEM
Noise Reduction = Pixel Avg.
System Vacuum = 9.14e-007 mbar
ZEISS

(b)

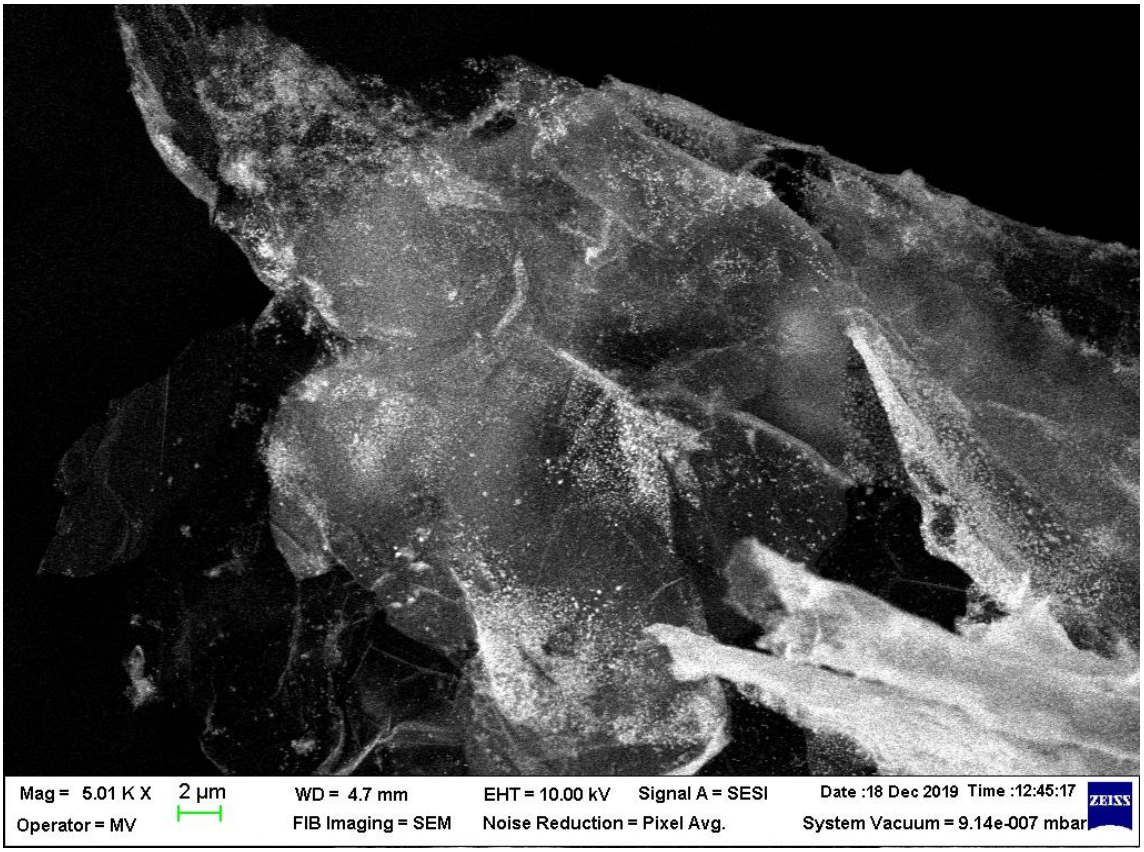
Mag = 5.01 K X
2 µm
WD = 4.7 mm
EHT = 10.00 kV
Signal A = SESI
Date :18 Dec 2019 Time :12:45:17
Operator = MV
FIB Imaging = SEM
Noise Reduction = Pixel Avg.
System Vacuum = 9.14e-007 mbar
ZEISS

(c)

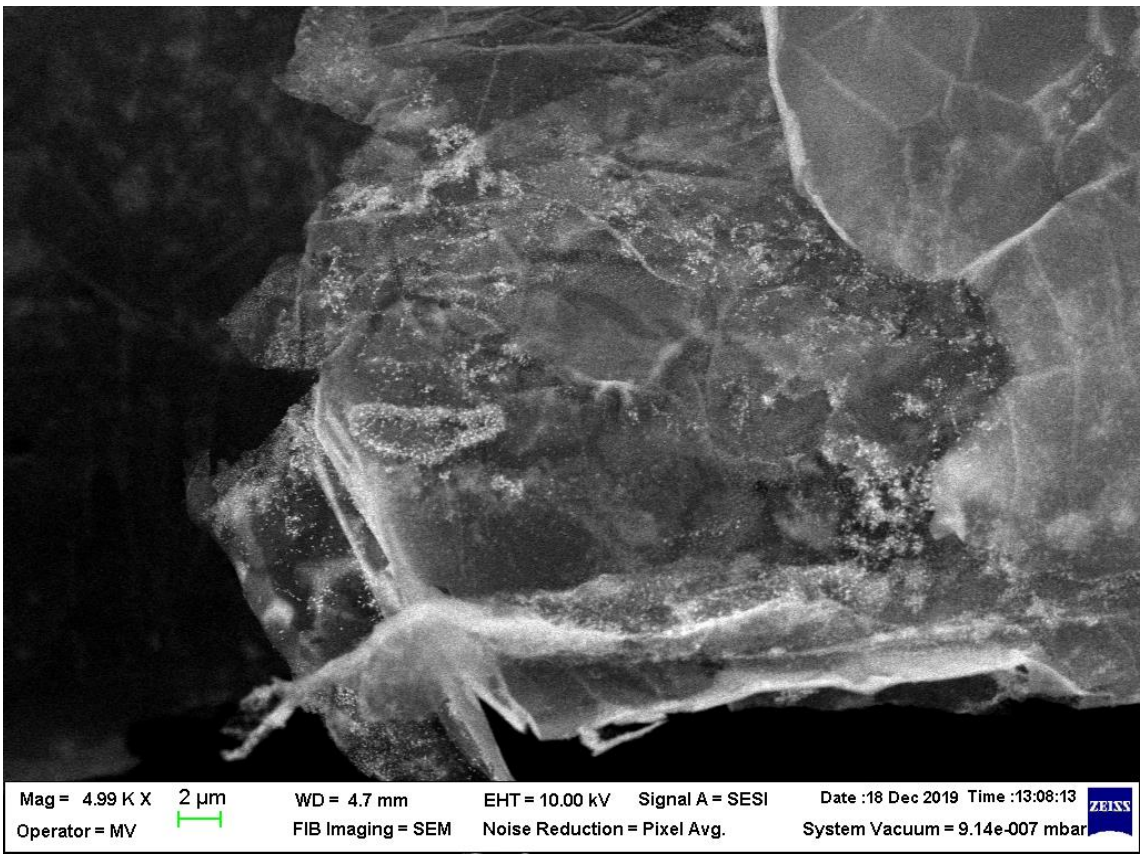
Mag = 4.99 K X
2 µm
WD = 4.7 mm
EHT = 10.00 kV
Signal A = SESI
Date :18 Dec 2019 Time :13:08:13
Operator = MV
FIB Imaging = SEM
Noise Reduction = Pixel Avg.
System Vacuum = 9.14e-007 mbar
ZEISS

(d)

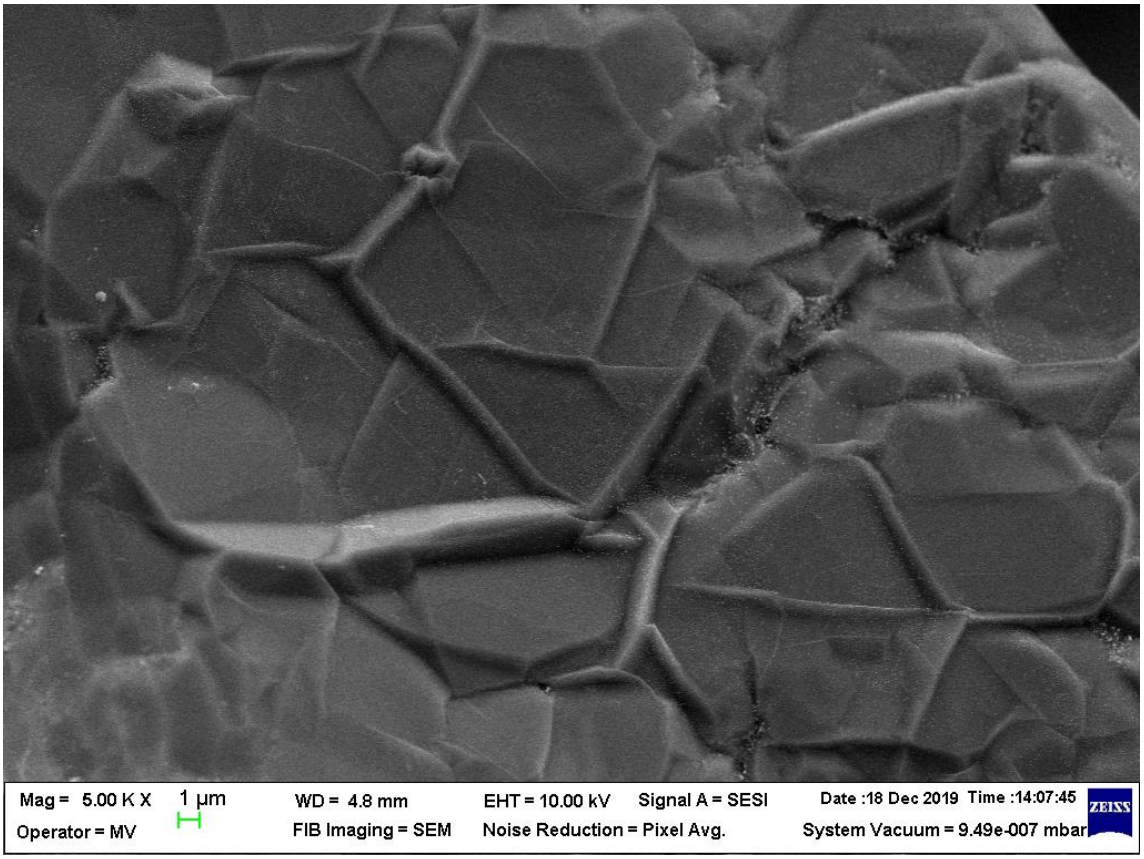

(e)

Fig. 2. SEM images of freestanding graphene networks obtained at different growing time after Ni removal: a) GN5, b) GN7, c) GN10, d) GN15, e) GN30

The presence of wrinkles in the images is a typical characteristic for graphene. Fig. 2e is a suggestive image (5000 X magnification) revealing the wrinkles at the grain boundaries of the graphene flakes. The graphene layers are smooth, and continuous, with very few cracks. We can see in Figs. 2a, 2b, 2c, 2d that some areas of the graphene are almost transparent in electron beam because the graphene sheet is very thin (few layers) and highly conductive.

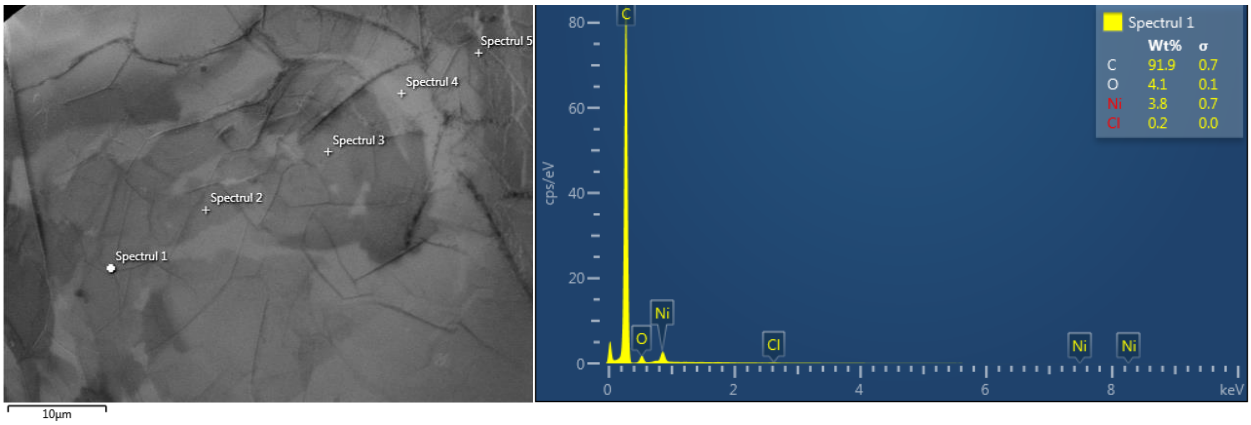

(a)

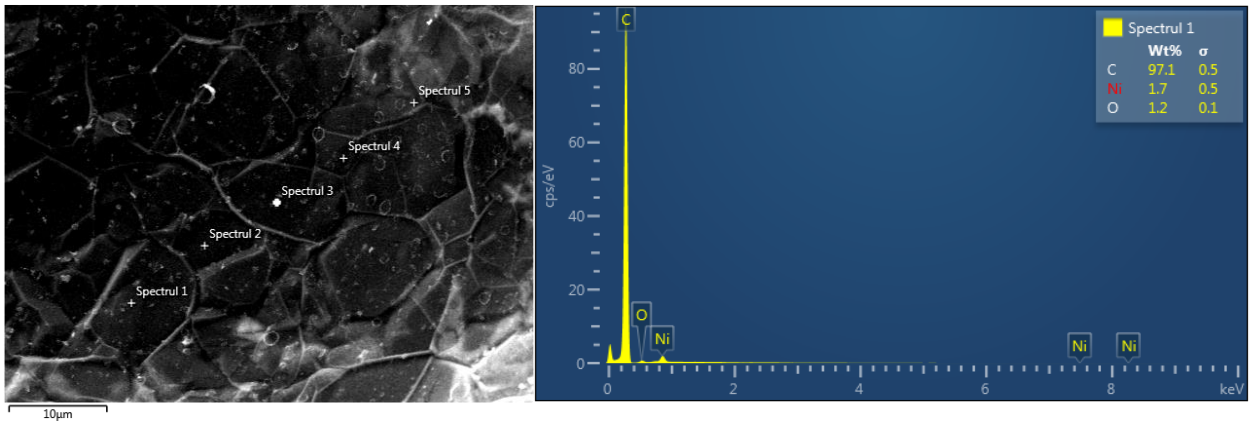

(b)

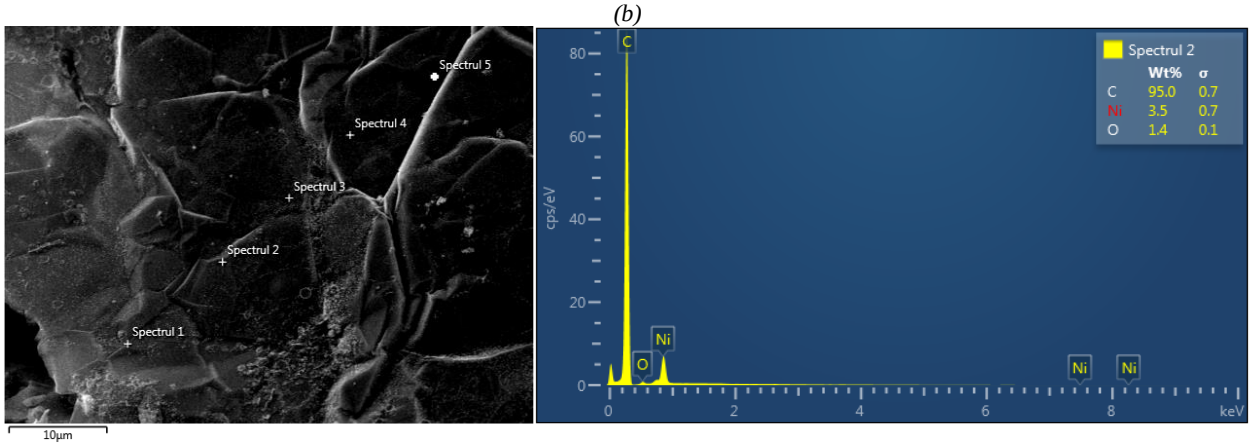

(c)

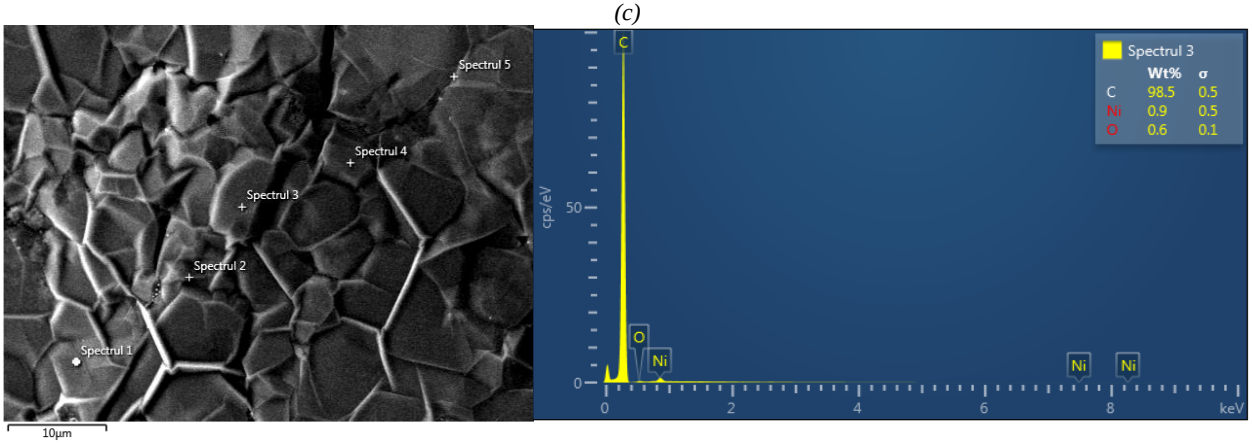

(d)

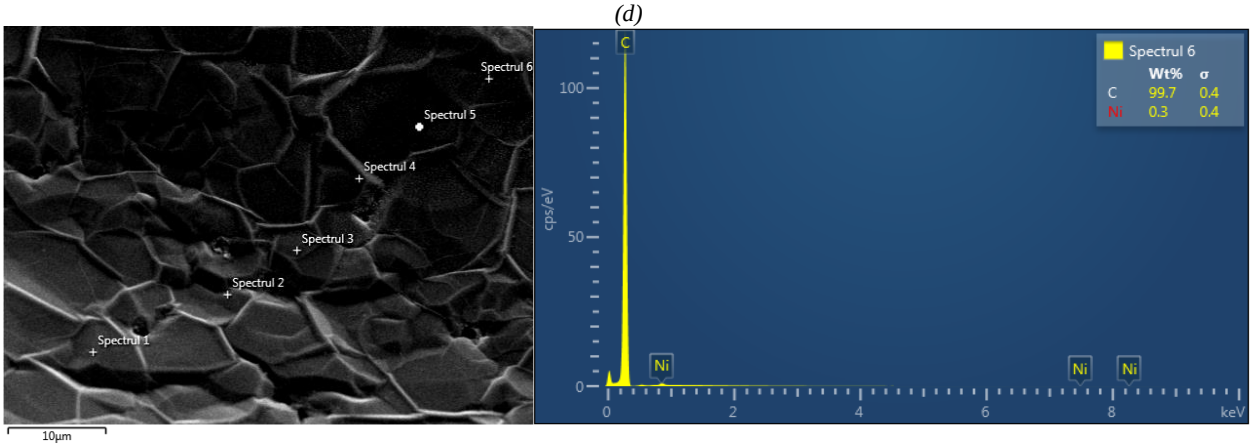

(e)

Fig. 3. EDS spectra of freestanding graphene networks after Ni removal: a) GN5, b) GN7, c) GN10, d) GN15, e) GN30 (color online)

Small traces of nickel were observed in the GN even if prolonged etching was performed, and this is evident in the EDS analysis presented in the Fig. 3 (a-e). The maximum quantity of nickel determined after the multipoint EDS analysis is 3.8% wt., as shown in the Fig. 3.

Fig. 4 presents the diffraction patterns of the GN obtained on Ni foam at different deposition times, after Ni etching.

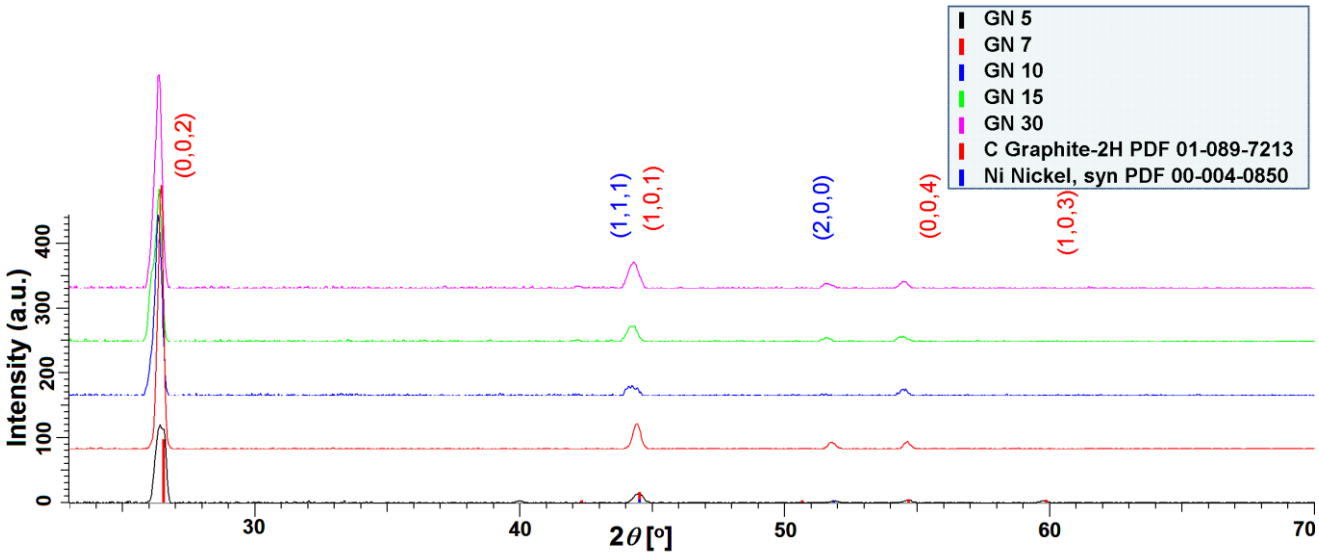

Fig. 4. XRD patterns of freestanding graphene networks obtained on Ni foam by CVD at different deposition times, after Ni etching (GN5, GN7, GN10, GN15, GN30) (color online)

The XRD patterns show the main characteristic peaks (002), (101) and (004) corresponding to the carbon presented as hexagonal graphite structure. The (002) reflection of the graphene samples appears at 2θ~26.5° with high intensity and sharpness, with the exception of the GN5 sample where the graphene sheet is very thin and the quantity of sample is very low. Increasing the growth time leads to the increase of the (002) peak intensity, the reduction of the Full Width at Half Maxima (FWHM), and a slight displacement of carbon (002) peak to lower angles, with the exception of the sample GN7. In any case, these characteristics do not have a linear evolution dependent on the deposition time of graphene. There are many factors that influence them, such as the structure of graphene, the thickness of graphene sheets (number of layers), and their orientation, taking into account the fact that we have a three-dimensional structure [28].

XRD patterns also reveal characteristic peaks of nickel (111) and (200) with very low intensity, which confirms the presence of small amounts of Ni in the freestanding graphene samples, also confirmed by the EDS analysis.

The Raman spectra of freestanding graphene networks obtained at different growing time are presented in figure 5. The spectra present the Raman bands characteristic to graphite-based materials [29, 30]: D (~1350 cm^{-1}), G (~1575 cm^{-1}) and 2D band (~2700 cm^{-1}), respectively. The D peak is associated with sp^3-hybridized carbon, showing defects or impurities in carbon materials, the G peak is assigned to the bond stretching of the pairs of sp^2 graphitic carbon atom, and the 2D peak corresponds to the high-energy second-order process [30]. The D peak intensity is very low (I_D/I_G~0.1), this fact indicating a small quantity of defects in the graphene structure, meaning a high-quality graphene.

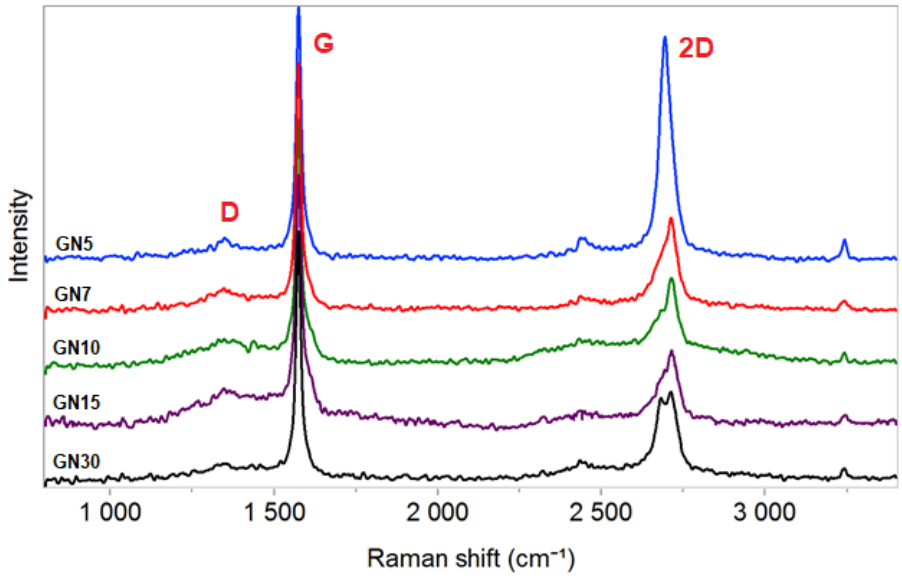

Fig. 5. Raman spectra recorded on freestanding graphene networks obtained at different growing time after Ni removal: GN5, GN7, GN10, GN15, GN30 (color online)

Table 1 presents the values of the Raman peaks of D, G and 2D band obtained for freestanding graphene networks, the ratio of the peak intensities I_D/I_G, I_{2D}/I_G and the number of the graphene layers estimated based on the value of I_{2D}/I_G ratio.

Table 1. Raman peaks of D, G and 2D band obtained for freestanding graphene networks

Sample	D	G	2D	I_D/I_G	I_{2D}/I_G	Number of graphene layers
GN5	1349	1575	2695	0.08	0.88	FLG
GN7	1353	1574	2712*	0.12	0.37	MLG
GN10	1347	1575	2715*	0.11	0.32	MLG
GN15	1346	1575	2716*	0.13	0.29	MLG
GN30	1344	1574	2712*	0.07	0.35	MLG

* 2D band splitting in two peaks

Note: $I_{2D}/I_G \geq 2$ - Single Layer Graphene (SLG); 1 - Double Layer Graphene (DLG); 0.5-0.8 - Few Layer Graphene (FLG), < 0.5 - Multi Layer Graphene (MLG) [28]

In the case of GN5 sample, the 2D band is a single intense peak at ~2695 cm^{-1}. For the other samples (GN7-GN30), the 2D band exhibits a multi-peak structure with two main intensities at ~2695 cm^{-1} and ~2712-2716 cm^{-1}. The 2D band splitting in two peaks for multilayer graphene networks appears probably due to the charging of the graphene layer [29]. The splitting of the 2D band is accentuated with the increase of the number of graphene layers from monolayer to multilayer, being more obvious for the GN30 sample.

The highest value of the I_{2D}/I_G ratio is presented by the GN5 sample (I_{2D}/I_G=0.88), this value indicating a few-layer graphene structure [28-30]. The other samples have a value of the I_{2D}/I_G ratio <0.37, indicating a multilayer graphene structure [31-33].

In their research paper, Cancado et al. [34] presented a set of empirical formulas that can be used to quantify the amount of point-like defects n_D (2), as well as to evaluate the average distance between these defects L_D (3), when using any energy/wavelength of the excitation laser in the visible range. According to the authors, equation (3) is valid only for Raman data obtained from graphene samples with point-like defects separated by $L_D \geq 10$ nm [34].

$$L_a\left(nm\right) = \left(2.4\times10^{-10}\right)\lambda_L^4\left(\frac{I_D}{I_G}\right)^{-1} \quad (1)$$

$$n_D(cm^{-2}) = \frac{\left(1.8\pm0.5\right)\times10^{22}}{\lambda_L^4}\left(\frac{I_D}{I_G}\right) \quad (2)$$

$$L_D^2\left(nm^2\right) = \left(1.8\pm0.5\right)\times10^{-9}\lambda_L^4\left(\frac{I_D}{I_G}\right)^{-1} \quad (3)$$

where:

L_a - the average nanocrystallite size, nm;

n_D - the amount of point-like defects, cm^{-2};

λ_L - the excitation laser wavelength (in our case is λ_L 532.06 nm);

L_D - the average size between two point-like defects in nanocrystalline graphene.

Using the three equations above (1-3), the L_a, n_D and L_D parameters were evaluated for all analyzed samples, the results being presented in Table 2.

Table 2. The L_a, n_D and L_D parameters values of the freestanding graphene networks

Sample	L_a (nm)	$n_D x 10^{10}$ (cm^{-2})	L_D (nm)
GN5	240	1.8	42
GN7	160	2.7	35
GN10	174	2.5	36
GN15	148	2.9	33
GN30	274	1.6	45

As it can be observed the GN 30 sample presents the highest value of the average crystallite size (274 nm), with the smallest amount of point-like defects and the largest average size between two point-like defects (45 nm). This is probably due to the fact that the graphene sheet has a higher thickness, thus it better maintains its structural integrity during the etching process of the nickel foam substrate.

4. Conclusions

The freestanding graphene networks were synthesized by CVD process with methane as carbon source using different deposition times (5, 7, 10, 15, and 30 minutes) and nickel foam as catalyst substrate.

SEM investigations revealed the specific structure of graphene with wrinkles at the grain boundaries of the graphene flakes. The graphene layers were smooth, and continuous, with very few cracks. Small traces of nickel were observed in the GN even if prolonged etching was performed.

The XRD patterns reveal the main characteristic peaks corresponding to the carbon, and some characteristic peaks of nickel with very low intensity, which confirms the presence of small amounts of Ni in the freestanding graphene samples, in good agreement with the EDS analysis.

According to the Raman spectra, we can conclude that the number of layers increases with the growing time. A high-quality freestanding graphene network with few-layer structure was synthesized at a deposition time of 5 minutes. The other samples obtained at a higher deposition time presented a multilayer structure.

The obtaining of a controlled number of layers is an important aspect for the integration of these three-dimensional graphene in different devices. Thus, this study provides us important information regarding the micro and macrostructure of three-dimensional graphene depending on the deposition time, so that we have the possibility to obtain three-dimensional graphene structures appropriate for a certain application like dye sensitized solar cells or carbon-based photodetectors. In conclusion, the graphene structure GN15 is most suitable for such applications because it is sufficiently thin and the macrostructure does not deteriorate after the removal of nickel in hydrochloric acid.

Acknowledgments

This work has received funding from the ATTRACT project funded by the EC under Grant Agreement 777222. The authors also acknowledge the financial support of the Romanian Ministry of Research and Innovation (MCI) through the contract no. 30 PFE/2018 and the Bilateral Collaboration Romania-Russia, project position 35 from the JINR Order no. 269/20.05.2020.

References

[1] S. M. Paek, E. Yoo, I. Honma, Nano Lett. **9**, 72 (2009).
[2] H. Wang, Q. Hao, X. Yang, L. Lu, X. Wang, Electrochem. Commun. **11**, 1158 (2009).
[3] C. Liu, S. Alwarappan, Z. Chen, X. Kong, C. Z. Li, Biosens. Bioelectron. **25**, 1829 (2010).
[4] R. I. Jafri, N. Rajalakshmi, S. Ramaprabhu, J. Mater. Chem. **20**, 7114 (2010).
[5] A. Petris, I. C. Vasiliu, P. Gheorghe, A. M. Iordache, L. Ionel, L. Rusen, S. Iordache, M. Elisa, R. Trusca, D. Ulieru, S. Etemadi, R. Wendelbo, J. Yang, K. Thorshaug, Nanomaterials **10**(9), 1638 (2020).
[6] L. Baschir, D. Savastru, A. A. Popescu, I. C. Vasiliu, M. Filipescu, A. M. Iordache, M. Elisa, S. M. Iordache, O. Buiu, C. Obreja, J. Optoelectron. Adv. M. **21**(7-8), 524 (2019).
[7] L. Baschir, A. M. Iordache, D. Savastru, A. A. Popescu, I. C. Vasiliu, M. Elisa, C. Obreja, M. Filipescu, R. Trusca, M. Stchakovsky, S. Iordache, J. Vac. Sci. Technol. B, **37**(6), 061208 (2019).
[8] Z. Chen, L. Jin, W. Hao, W. Ren, H.-M. Cheng, Mater. Today Nano **5**, 100027 (2019).
[9] R. M. Firdaus, N. Berrada, A. Desforges, A. R. Mohamed, B. Vigolo, Chem. Asian J. **15**, 2902 (2020).
[10] X. H. Cao, Z. Y. Yin, H. Zhang, Energy Environ. Sci. **7**, 1850 (2014).
[11] V. Chabot, D. Higgins, A. Yu, X. Xiao, Z. Chen, J. Zhang, Energy Environ. Sci. **7**, 1564 (2014).
[12] Y. Ma, Y. Chen, Natl. Sci. Rev. **2**, 40 (2015).
[13] Y. Zhang, Q. Wan, N. Yang, Small **15**, 1903780 (2019).
[14] X. T. Zhang, Z. Y. Sui, B. Xu, S. Yue, Y. Luo, W. Zhan, B. Liu, J. Mater. Chem. **21**, 6494 (2011).
[15] M. A. Worsley, P. J. Pauzauskie, T. Y. Olson, J. Biener, J. H. Satcher Jr., T. F. Baumann, J. Am. Chem. Soc. **132**, 14067 (2010).
[16] Z. Chen, W. Ren, L. Gao, B. Liu, S. Pei, H. Cheng, Nat. Mater. **10**, 424 (2011).

[17] X. Xie, Y. Zhou, H. Bi, K. Yin, S. Wan, L. Sun, Sci. Rep. **3**, 2117 (2013).
[18] H. Bi, X. Xie, K. Yin, Y. Zhou, S. Wan, L. He, F. Xu, F. Banhart, L. Sun, R. S. Ruoff, Adv. Funct. Mater. **22**, 4421 (2012).
[19] Y. Geng, Z. Li, M. Chen, H. Zhao, L. Zhang, J. Sol-Gel Sci. Technol. **94**, 375 (2020).
[20] L. M. Veca, F. Nastase, C. Banciu, M. Popescu, C. Romanitan, M. Lungulescu, R. Popa, Diam. Relat. Mater. **87**, 70 (2018).
[21] F. Yavari, Z. Chen, A. V. Thomas, W. Ren, H. M. Cheng, N. Koratkar, Sci. Rep. **1**, 166 (2011).
[22] Y. Shen, Q. Fang, B. Chen, Environ Sci. Technol. **49**, 67 (2015).
[23] M. Xiao, T. Kong, W. Wang, Q. Song, D. Zhang, Q. Ma, G. Cheng, Adv. Funct. Mater. **25**, 6165 (2015).
[24] E. Chitanu, C. Banciu, G. Sbarcea, V. Marinescu, A. Bara, P. Barbu (Prioteasa), Rev. Chim. **69**, 3376 (2018).
[25] K. Lee, J. Lee, K. W. Kwon, M. S. Park, J. H. Hwang, K. J. Kim, ACS Appl. Mater. Interfaces **9**, 22502 (2017).
[26] M. Pettes, R. H. Ji, L. Shi, Nano Lett. **12**, 2959 (2012).
[27] C. Banciu, M. Lungulescu, A. Bara, L. Leonat, A. Teisanu, Optoelectron. Adv. Mat. **11**(5-6), 368 (2017).
[28] M. Shiraishi, M. Inagaki, Carbon Alloys, Novel Concepts to Develop Carbon Science and Technology, 161 (2003)
[29] A. C. Ferrari, Solid State. Comm. **143**, 47 (2007).
[30] F. Tuinstra, J. L. Koenig, J. Chem. Phys. **53**, 1126 (1970).
[31] S. Gayathri, P. Jayabal, M. Kottaisamy, V. Ramakrishnan, AIP Adv. **4**, 027116 (2014).
[32] X. Wang, J. W. Christopher, A. K. Swan, Sci. Rep. **7**, 13539 (2017).
[33] H. Kato, N. Itagaki, H. J. Im, Carbon **141**, 76 (2019).
[34] L. G. Cancado, A. Jorio, E. H. Martins Ferreira, F. Stavale, C. A. Achete, R. B. Capaz, M. V. O. Moutinho, A. Lombardo, T. S. Kulmala, A. C. Ferrari, Nano Lett. **11**, 3190 (2011).

*Corresponding author: cristina.banciu@icpe-ca.ro